2015 IEEE/RSJ International Conference on Intelligent Robots and Systems (IROS)
Congress Center Hamburg
Sept 28 - Oct 2, 2015. Hamburg, Germany

Design of Low Inertia Manipulator with High Stiffness and Strength Using Tension Amplifying Mechanisms

Yong-Jae Kim

Abstract— **This paper presents a novel manipulator for human-robot interaction that has low mass and inertia without losing stiffness and payload performance. A lightweight tension amplifying mechanism that increases the joint stiffness in quadratic order is proposed. High stiffness is essential for precise and rapid manipulation, and low mass and inertia are important factors for safety due to low stored kinetic energy. The proposed tension amplifying mechanism was applied to a 1-DOF elbow joint and then extended to a 3-DOF wrist joint. The developed manipulator was analyzed in terms of inertia, stiffness, and strength properties. Its moving part weighs 3.37 kg, and its inertia is 0.57 kg·m^2, which is similar to that of a human arm. The stiffness of the developed elbow joint is 1440Nm/rad, which is comparable to that of the joints with rigid components in industrial manipulators. A detailed description of the design is provided, and thorough analysis verifies the performance of the proposed mechanism.**

I. Introduction

SAFETY and performance are the key features for robot manipulators as well as targets to be traded off [1,2]. As the efforts to detect external force and collisions by using sensors, various types of manipulators with joint torque sensors or force-torque sensors have been developed. For instance, KUKA LWR equipped with integrated joint torque sensors shows excellent force control characteristics due to its precise sensors and accurate modeling [3]. However, its mechanical properties are more similar to industrial robots than human arms, and thus, inherent safety against collision and impact is hard to achieve without exhaustive feedback control under relatively low speed.

In order to enhance the capability of physical human-robot interaction into the inter-human interaction level, a collision should be treated not only as an object to be absorbed or mitigated but also as the means for communication and cooperation. For inherent safety, mechanically compliant manipulators have been investigated for several decades. One of the most popular approaches is series elastic actuator (SEA), which has a constant spring between its actuator output and robotic link [4]. While it remedies the high impedance of the actuators, it has the drawback of low stiffness and limited bandwidth that leads to degraded position control performance [1]. Recently, manipulators with variable stiffness joints (VSJs) are widely investigated because they can achieve both the safety of SEA and the control performance of conventional rigid joints [5]. But stiffness adjusting mechanisms increase the mechanical complexity and corresponding mass, which undermines the human-like inherent safety. Gravity compensation mechanisms and clutch mechanisms [6,7] are also highly effective ways to limit the excessive force to environments; however, they tend to be complex and bulky as are VSJs.

Yong-Jae Kim is with Koreatech (Korea University of Technology and Education), Chungjeol-Ro, Byeongcheon-Nyeon, Dongnam-Gu, Cheonan City, Chungnam Province, Rep. of Korea. (phone: +82-41-560-1424, e-mail: yongjae@koreatech.ac.kr)

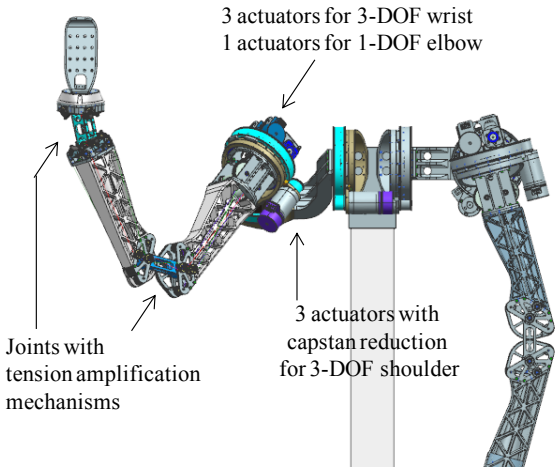

Fig. 1. LIMS (Low Inertia Manipulator with High Stiffness and Strength) that has extremely low inertia and mass comparable to humans

Lightweight design with high backdrivability can be considered as the ultimate approach to human-like manipulators. The lightweight mechanism guarantees safety at high speed because the stored kinetic energy is small. In a strict sense, the rotational inertia of the links including the reflected motor and gear inertia rather than mass must be taken into account in order to consider stored kinetic energy of the rotational joint. The tendon transmission mechanism is widely used to reduce the inertia by placing heavy actuators at the proximal part [8, 9]. Moreover, the tendon also can be used as a reduction mechanism with negligible backlash and low friction. However, the low stiffness and limited strength of tendon also greatly decreases the control performance and maximum payload.

This paper presents a 7-DOF manipulator named LIMS (Low Inertia Manipulator with high Stiffness and Strength), as shown in Fig. 1. Four motors for the elbow and wrist are mounted at the shoulder part, and tendons transmit the motor motion to the wrist and elbow at the distal part, similar to other tendon-driven manipulators. But a unique light-weight tension

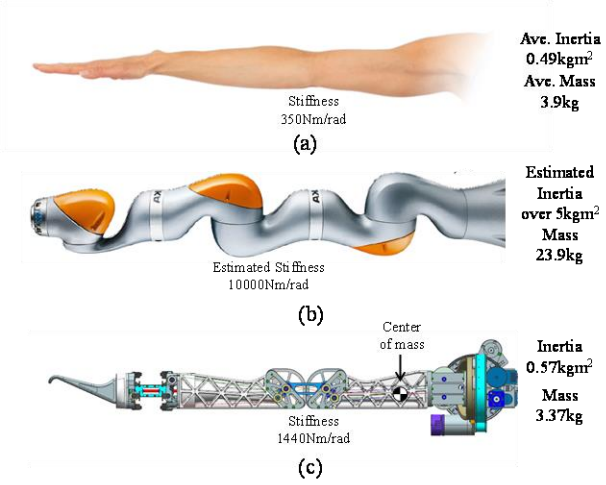

Fig. 2. Mechanical properties. (a) A human arm, (b) KUKA LBR iiwa, (c) Proposed manipulator LIMS

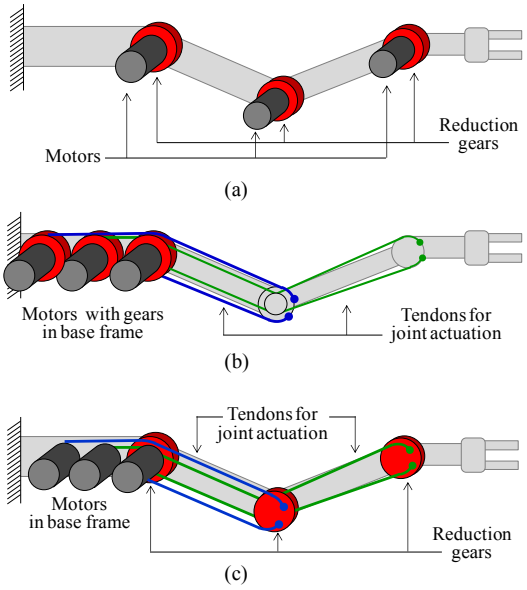

Fig. 3. Conceptual structures of manipulators. (a) a conventional industrial robot, (b) a tendon driven manipulator, (c) an example of a hybrid structure

amplifying mechanisms regain the joint stiffness in quadratic order without increasing mass and inertia.

The paper is structured as follows. In Section II, the design philosophy is introduced considering safety and performance metrics. Section III describes the basic mechanics of tension amplification mechanism and the mechanical design of the proposed manipulator in detail. In Sections IV and V, stiffness and strength properties are analyzed and validated. Section VI presents conclusions and future work.

II. Design Requirements Based on Safety and Performance Metrics

Even though many manipulators have been investigated, as mentioned in Section I, they cannot match the safety and performance of human arms. Clapping, hugging, patting, and even giving a high five are natural and easy with human arms but extremely difficult and dangerous for robotic arms. It is obvious that these differences do not solely come from the sensor performance or control algorithms. Figs. 2(a) and (b) show a wide difference in the mass, inertia, and stiffness between a human arm and the robotic arm KUKA LBR iiwa. The inertia of the LBR iiwa is approximately 10 times higher than that of a human.

Various safety metrics in human-robot interaction have been investigated and suggested over several decades. Head Injury Criterion (HIC) is a well-known and widely-used metric. HIC is derived from the average acceleration of a human head and the applied time. Other criteria, like ISO10218, limit maximum speed (0.25m/s), power (80W), or force (150N). Most of these criteria indicate that decreasing the total energy transferred to humans and increasing the transferring time are the most effective ways to reduce injury. A compliant covers can be a simple and effective solution by increasing the energy transferring time but cannot be the primary means of achieving safety. For instance, the PUMA robot, with a speed of 1m/s needs more than 127mm thickness of soft cover to satisfy HIC100 [1]. Thus, decreasing the total transferring energy by minimizing robot inertia can be considered as the fundamental way of reducing injury and even utilizing impact as communication and collaboration with humans.

On the other hand, high stiffness and strength are essential properties of manipulator performance. Especially, stiffness is critical for control speed and tracking performance because it determines system bandwidth. Measurement of the stiffness of human joints is still a contentious issue, and [10] reported that the stiffness of the human elbow joint is about 350Nm/rad, which is small (joint stiffness of KUKA LBR iiwa is about 10000 Nm/rad) but substantially greater than other tendon driven manipulators (joint stiffness of [8] is 35Nm/rad).

Consequently, in order to develop an inherently safe manipulator without losing performance, the following design requirements were established.

1) Extremely low inertia to minimize stored kinetic energy.
2) Extremely low mass. Conventional industrial robots consume substantial amount of the motor torque in supporting their own weight.
3) High stiffness comparable to industrial robots.
4) High payload comparable to industrial robots.
5) Efficiency and backdrivability. In order to apply the right amount of energy to the robot, an efficient mechanism with minimal frictional loss is required. Moreover, high back -drivability enables the sensing of external force without expensive force or torque sensors.

Fig. 3 illustrates configurations of motors, gears, and the links for several types of manipulators. Fig. 3 (a) shows the typical configuration of industrial robots that have heavy weight due to heavy components like motors and gears at the distal part. Fig. 3 (b) is a common configuration of a

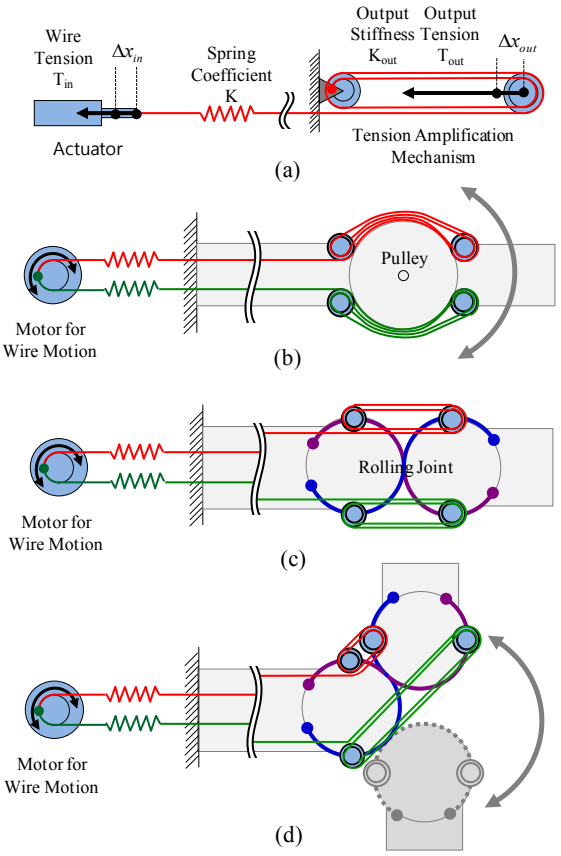

Fig. 4. Conceptual design of 1-DOF tension amplifying mechanism

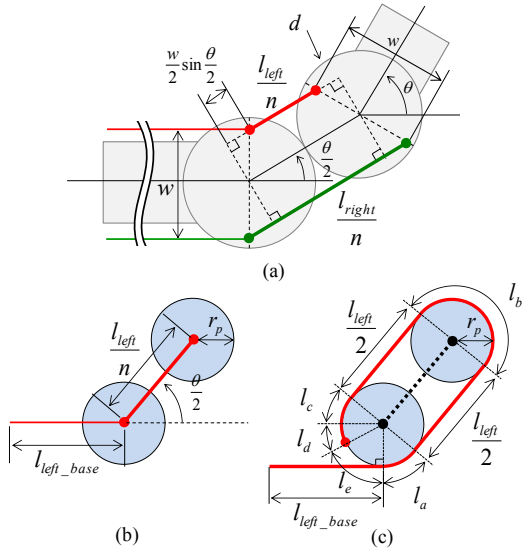

Fig. 5 The relationship between the wire motion and the joint angle

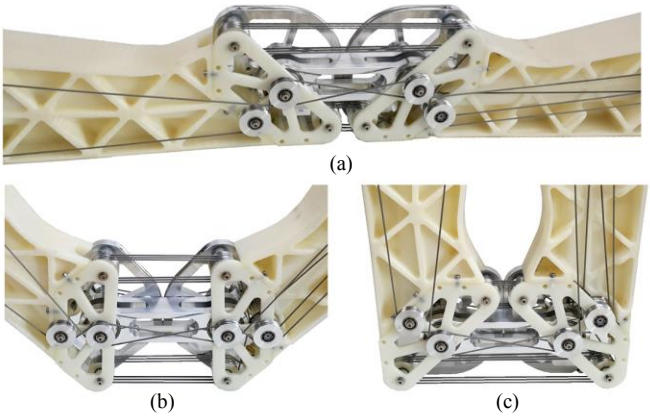

Fig. 6 Implemented elbow joint (a) straight pose ($\theta = -90\,\text{deg}$), (b) center of ROM ($\theta = 0\,\text{deg}$), and (c) fully bent pose ($\theta = 90\,\text{deg}$).

tendon-driven manipulator where the motors and gears are at the proximal part. As previously mentioned, the elasticity and limited strength of tendons cause low stiffness and strength of the robot. If high payload wires with large diameter are used to improve stiffness and strength, the mechanism will become complicated and bulky because the wires need a large bending radius and large-size pulleys and also the frame must withstand the compression caused by the high tension.

Fig. 3(c) is a trade-off between (a) and (b), and it has several advantages over (b). It has low mass and inertia compared to (a). Moreover, the reflected joint stiffness caused by tendons is amplified in the quadratic order, which will be explained in the next section. However, the inertia is still substantial because of the heavy gears at the distal part, and the tendon mechanism for multiple DOF joints is difficult to implement. Therefore, a new lightweight transmission and reduction mechanism is required.

III. Mechanical Design of LIMS

A. One-DOF Tension Amplifying Mechanism

Fig. 4(a) shows the basic concept of a simple tension amplification mechanism. An actuator on the left side is connected by a tendon with a reduction mechanism, which is composed of fixed and movable pulleys, a so-called "block and tackle". If the wire tension exerted by the actuator is T_{in} and the number of wire turns around the pulleys is n (in Fig. 4(a), $n = 4$), the resultant tension T_{out} by tension amplification mechanism is simply:

$$T_{out} = nT_{in} \,, \tag{1}$$

where it is assumed that the friction in this mechanism is negligible. If we consider the reduction of motion, the output motion Δx_{out} is n times smaller than actuator motion Δx_{in}, i.e. $\Delta x_{out} = \Delta x_{in} / n$. Therefore, the resultant stiffness of the tension amplifying mechanism is

$$K_{out} = \frac{T_{out}}{\Delta x_{out}} = \frac{nT_{in}}{\Delta x_{in} / n} = n^2 K \,, \tag{2}$$

where K denotes the spring coefficient of the whole wire. This shows that the mechanism amplifies the tension in quadratic order. For revolute motion of a robotic joint, a pair of the tension amplifying mechanism shown in Fig. 4 (b) is required to form antagonistic wire motion. The pulley at the center of the joint makes the agonistic and antagonistic wire motions symmetric. Without this pulley, the wire motions will not be symmetrical, and thus, the sum of the wire lengths will differ, which means that an individual motor for each wire is needed.

By adopting a rolling joint as in Fig. 4(c), the motions of the wire pair become symmetrical, and the range of motion can be larger (compare Figs. 4(d) with (b)). The two rolling surfaces have a circular part, and two additional wires (blue and purple wires in the figure) prevent slipping and enable pure rolling. It can be replaced with the gear teeth for miniaturization such as surgical instruments. For further details on this application, refer to [11].

The relationship between the wire motion and the joint angle can be derived from Fig. 5 (a), where the fixed and movable pulleys were omitted for ease of explanation. In this figure, l_{left}, l_{right}, d, w, and θ denote the total lengths of the agonistic and antagonistic wires wound between the two centers of pulleys, diameter of the rolling surface, width between the agonistic-antagonistic pulley centers, and the bending angle, respectively. If the joint is in a straight pose ($\theta = 0$), l_{left} and l_{right} have the same length nd where the amplification number n is the number of wire turns around the pulleys, as previously described. In the case of bending, the two lengths are obtained as follows:

$$l_{left} = n\left(d - w\sin\frac{\theta}{2}\right),\ l_{right} = n\left(d + w\sin\frac{\theta}{2}\right). \quad (3)$$

If we consider only the amount of wire movement of (3),

$$\Delta l_{left} = -\Delta l_{right} = nw\sin\frac{\theta}{2}. \quad (4)$$

This confirms that the motion of wire pair is fully symmetrical and simple actuation mechanism with one motor is applicable. (3) and (4) were derived with the simplified model by ignoring the diameter of the fixed and moving pulleys. Fig. 5 (b) and (c) illustrate the simplified and actual wire paths, respectively. Assuming an even number of n (here, $n = 2$), the actual wire length is

$$\begin{aligned} l_{total} &= l_{left\_base} + l_a + l_{left}/2 + l_b + l_{left}/2 + l_c + l_d \\ &= l_{left\_base} + l_{left} + \left(2\pi r_p - l_d\right) \end{aligned}. \quad (5)$$

Therefore, the wire movement Δl_{left} of the actual wire path is exactly the same as the simplified path if the wire end is fixed on the proximal rolling surface frame, and thus, l_d is constant because the only variable in the last term of (5) is l_{left}. It is valid for every even number of n. To sum up, by setting n as an even number and fixing the wire end on the proximal frame, the actual wire movement agrees with (4).

Fig. 6 illustrates the implemented elbow joint by using the proposed 1-DOF tension amplifying mechanism. The range of motion (ROM) is 180 deg, and the amplification number n is 6. As it is made of aluminum alloy and 3D-printed ABS material, it has substantially lower mass compared to that of conventional industrial manipulators. The mass and inertia distribution are described in detail in Section V.

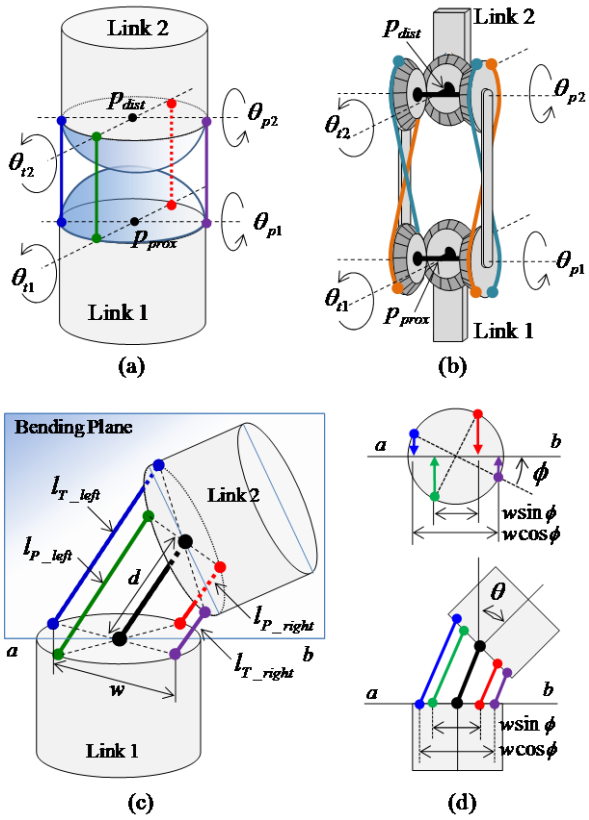

Fig. 7 Conceptual design of 2-DOF tension amplification mechanism

B. 2-DOF and 3-DOF Tension Amplifying Mechanism

Heretofore, a 1-DOF tension amplifying mechanism and the developed elbow joint were explained. For the wrist, high DOF joint can be constructed by connecting the multiple proposed 1-DOF mechanisms in serial; however, the joint configuration can be unsuitable for dexterous manipulation, and the wire path can be overly complicated. Thus, a new way to extend the proposed concept is needed without sacrificing the tension amplifying property, wide range of motion, simplicity, and so on.

Fig. 7 (a) briefly illustrates an extended concept of the tension amplifying mechanism. There are two hemispherical rolling surfaces instead of the circular-shaped part that are surrounded by two wire pairs for 2-DOF pan-tilt motion. But this is almost infeasible because the hemispheres occupy the wire path when bending and the contact point cannot endure slipping force and torsional force. Also, each wire pair must be verified to exhibit symmetric behavior, even under combined pan and tile motion.

In order to emulate spherical rolling contact, a unique coupling link is proposed, as shown in Fig. 7 (b). It is composed of two identical bevel gear sets and each bevel gear set is again composed of three bevel gears with equal numbers of teeth. The center gear is attached to the link, and the two side gears are coupled with the other side gears of the other bevel gear set with wires. Naming the pan and tilt angle between links 1 and 2 in Fig. 7 (b) as θ_p and θ_t, respectively,

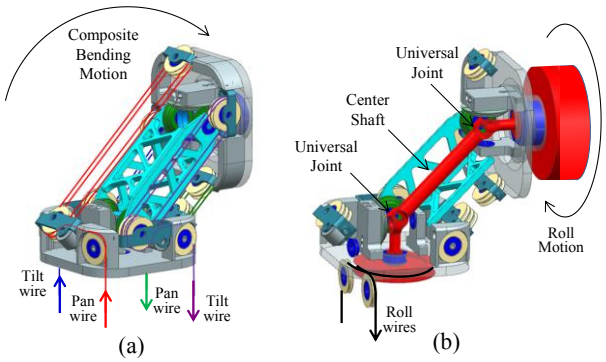

Fig. 8 Detail design of 3-DOF wrist joint

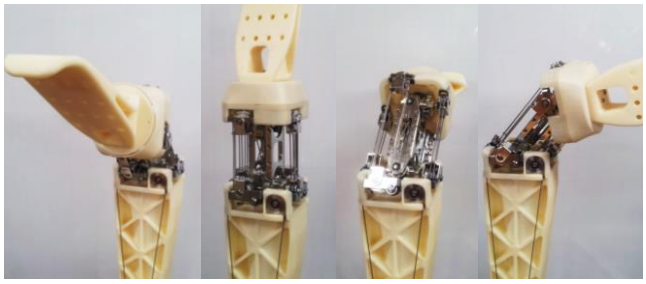

(a) (b) (c) (d)

Fig. 9 Implemented wrist joint

the proposed coupling mechanism satisfies the following motion as

$$\frac{\theta_p}{2} = \theta_{p1} = \theta_{p2}, \quad \frac{\theta_t}{2} = \theta_{t1} = \theta_{t2}, \tag{6}$$

which means that it has the same movement as spherical rolling contact motion.

Fig. 7 (c) illustrates an example of the bent pose. Here, we can assign a plane, called bending plane, where the two center lines of the cylinders of links 1 and 2 coexist. Fig.7 (d) shows the top view and the side view by projecting the wires to the bending plane, and ϕ denotes the angle between the panning axis and the bending plane. As can be seen in the side view at bottom part of Fig. 7 (d), the configurations of the two wire pairs are similar to the 1-DOF mechanism, except the width w between the pulley centers. The equivalent widths for the pan wire pair and tilt wire pair are $w\cos\phi$ and $w\sin\phi$, respectively. Therefore, substituting w of (4) with $w\cos\phi$ and $w\sin\phi$, the relationship between the bending pose (ϕ,θ) and the motion of wire pair $(\Delta l_p, \Delta l_t)$ can be obtained as the following equations and the wire movement of each wire pair is fully symmetric.

$$\begin{aligned} \Delta l_{P\_left} &= -\Delta l_{P\_right} = nw\sin\phi\,\sin\frac{\theta}{2} \\ \Delta l_{T\_left} &= -\Delta l_{T\_right} = nw\cos\phi\,\sin\frac{\theta}{2} \end{aligned} \tag{7}$$

In general, most robot wrists, as well as those of humans, have 3 DOF for dexterous manipulation. By utilizing the hollow space of the coupling mechanism, as in Fig. 7 (b), the 2-DOF tension amplifying mechanism can be extended to the 3-DOF mechanism. As shown in Fig. 8 (b), the center shaft and two universal joints transfer rotation motion to the distal end of the wrist, and totally 3-DOF wrist motion can be achieved. Fig. 9 shows the implemented 3-DOF wrist. The wrist can bend ±90 deg and rotate 720 deg. The wire tension was amplified by 4 times ($n = 4$).

IV. Stiffness And Strength Analysis

In this section, the stiffness and strength of the proposed tension amplifying mechanism are calculated. Here the stiffness and strength of the wires are considered, the friction of the mechanism is assumed to be negligible, and the stiffness and strength of frames or motors are sufficiently high to be treated as rigid bodies. This seems reasonable because the wire is the most dominant flexible component in the manipulator having limited breaking strength.

Let us consider (4) to obtain the tension-torque relationship of the 1-DOF joint. By using the virtual work concept, an energy conservation equation can be obtained as

$$\begin{aligned} \tau_{1DOF}\delta\theta &= T_{pulled}\delta(\Delta l) - T_{loosen}\delta(\Delta l) \\ &= \Delta T\delta(\Delta l) \end{aligned}, \tag{8}$$

where $\delta(\Delta l)$, $\delta\theta$, and τ_{1d} denote the infinitesimal changes of the wire motion Δl, the bending angle θ, and the resultant joint torque, respectively. ΔT means the difference of the tensions of pulled wire and loosen wire ($\Delta T = T_{pulled} - T_{loosen}$). Thus, it implies the force generated by the actuator, as shown in Figs. 4 (c) or (d). From (8) and the differentiated equation of (4), the joint torque can be calculated as follows:

$$\tau_{1DOF} = \frac{\delta(\Delta l)}{\delta\theta}\Delta T = \left(\frac{nw}{2}\cos\frac{\theta}{2}\right)\Delta T. \tag{9}$$

Therefore, considering maximum breaking strength of the wire $T_{\max}$, the maximum strength of the 1-DOF tension amplifying mechanism is obtained as follows:

$$\tau_{1DOF\max} = \left(\frac{nw}{2}\cos\frac{\theta}{2}\right)T_{\max}. \tag{10}$$

This shows that the maximum strength is proportional to the amplification number n and decreases as the joint angle θ goes away from zero.

The joint stiffness can be derived as follows. Assuming that the actuator is fixed at a certain angle θ and the infinitesimal external torque $\delta\tau$ is applied to the joint, let us consider the infinitesimal angle change $\delta\theta$ due to infinitesimal wire movement $\delta(\Delta l)$. From (9) and differentiated equation of (4),

$$\begin{aligned} \delta\tau &= \left(\frac{nw}{2}\cos\frac{\theta}{2}\right)\left(T_{pulled} - T_{loosen}\right) \\ &= \left(\frac{nw}{2}\cos\frac{\theta}{2}\right)\left(k(T_p + \delta(\Delta l)) - k(T_p - \delta(\Delta l))\right) \\ &= \left(\frac{nw}{2}\cos\frac{\theta}{2}\right)2k\delta(\Delta l) = \left(\frac{nw}{2}\cos\frac{\theta}{2}\right)2k\left(\frac{nw}{2}\cos\frac{\theta}{2}\right)\delta\theta \end{aligned}, \tag{11}$$

where k denotes the spring coefficient of each of the wire pairs under the assumption of approximately the same stiffness, and T_p means the pretension of the wires.

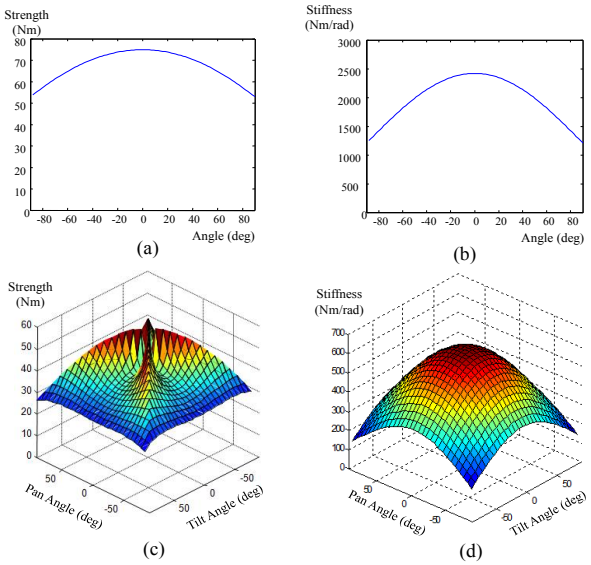

Fig. 10. (a) Strength of the 1-DOF mechanism, (b) stiffness of the 1-DOF mechanism, (c) strength of the 2-DOF mechanism, (d) stiffness of the 2-DOF mechanism

Consequently, the stiffness of the 1-DOF joint k_{1DOF} is

$$k_{1DOF} = \frac{\delta\tau}{\delta\theta} = \left(\frac{n^2 w^2}{2}\cos^2\frac{\theta}{2}\right)k. \qquad (12)$$

This verifies that the stiffness is proportional to the square of the amplification number n.

In order to extend these stiffness and strength properties of the 1-DOF mechanism into 2 DOF, consider the situation of Fig. 7 (d). Even though the stiffness and strength can be defined as two dimensional directions, we focus on the stiffness and strength in the banding plane for simplicity. The maximum strength of the 2-DOF mechanism can be calculated by adding the separated contribution of pan wire pair and tilt wire pair. In the case of $|\sin\phi| > |\cos\phi|$,

$$\begin{aligned}\tau_{2DOF\max} &= \tau_{\max\_Pan} + \frac{|\sin\phi|}{|\cos\phi|}\tau_{\max\_tilt} \\ &= \left(\frac{nw|\cos\phi|}{2}\cos\frac{\theta}{2}\right)T_{\max} + \frac{|\sin\phi|}{|\cos\phi|}\left(\frac{nw|\sin\phi|}{2}\cos\frac{\theta}{2}\right)T_{\max} \\ &= \frac{nw}{2}\frac{|\sin^2\phi| + |\sin^2\phi|}{|\cos\phi|}\cos\frac{\theta}{2}T_{\max} \\ &= \left(\frac{nw}{2|\cos\phi|}\right)\cos\frac{\theta}{2}T_{\max}\end{aligned}$$

where $T_{\max\_Pan}$ and $T_{\max\_Tilt}$ mean the maximum strength due to each wire, and these can be obtained by substituting w of (10) with $w\cos\phi$ and $w\sin\phi$. The contribution of the tilt wire is scaled down by $|\sin\phi|/|\cos\phi|$ because the tilt wire is not fully stretched from the breaking tension. Therefore, the resultant maximum strength is

$$\tau_{2DOF\max} = \left(\frac{nw}{2\max(|\cos\phi|,|\sin\phi|)}\cos\frac{\theta}{2}\right)T_{\max}. \qquad (13)$$

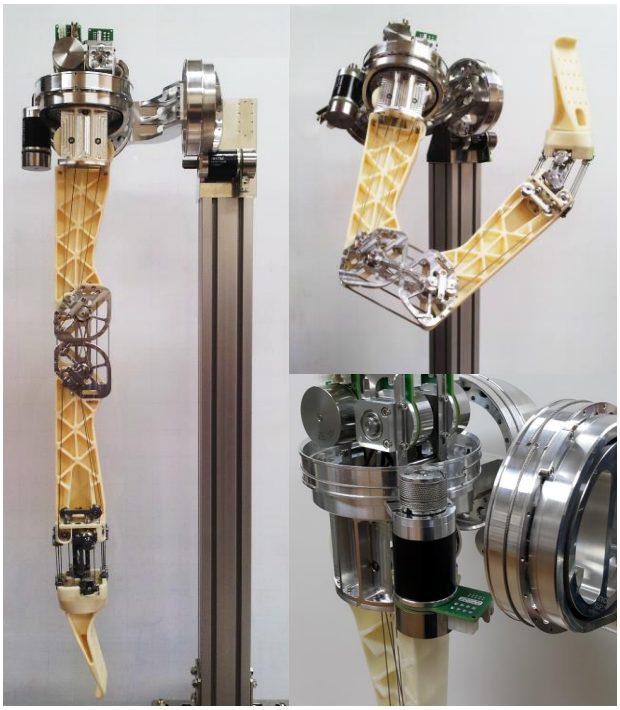

(a)

(b)

Fig. 11 (a) implemented robot LIMS, (b) motor and pulley reduction assembly for wrist and elbow actuation.

Similarly, the stiffness can be derived as follows:

$$\begin{aligned}k_{2DOF} &= k_{1DOF\_Pan} + k_{1DOF\_Tilt} \\ &= \left(\frac{n^2(w\cos\phi)^2}{2}\cos^2\frac{\theta}{2}\right)k + \left(\frac{n^2(w\cos\phi)^2}{2}\cos^2\frac{\theta}{2}\right)k\end{aligned}.$$

Consequently, the stiffness of the 2-DOF joint k_{2DOF} is

$$k_{2DOF} = \left(\frac{n^2 w^2}{2}\cos^2\frac{\theta}{2}\right)k. \qquad (14)$$

It is notable that the stiffness of the 2-DOF joint is not affected by the bending direction ϕ, which means that the wrist has the same stiffness regardless of the bending direction and it is beneficial to control performance. Fig. 10 illustrates the stiffness and strength changes of the 1-DOF and 2-DOF tension amplifying mechanism obtained from (10), (12), (13), and (14). Please note that the strength in this section is the maximum strength derived from wire breaking strength. Thus, the actual maximum strength, or payload, should be determined by considering this as well as maximum motor torque and motor driver performance.

TABLE I
DESIGN PARAMETERS

Items	Design Parameters	
	1-DOF Elbow	2-DOF Wrist
n	6	4
w	80 mm	67 mm
k	30 N/mm	24 N/mm
T_{max}	312 N	312 N

TABLE II
LIMS SPECIFICATIONS

Items		Specifications
Mass	upper arm	2.41 kg (moving part only)
	lower arm	0.64 kg
	wrist	0.32 kg
Inertia	shoulder-wrist	571,410 kg mm^2
	elbow-wrist	109,520 kg mm^2
	wrist only	30,960 kg mm^2
Equivalent gear ratio	shoulder	119.6:1
	elbow	88.2:1
	wrist	49.2:1
Max torque	shoulder	peak 71.9Nm, cont. 16.6Nm
	elbow	peak 48.8Nm, cont. 11.2Nm
	wrist	peak 12.5Nm, cont. 4.1Nm
Stiffness	elbow	Calculated : 2,420 Nm/rad Measured : 1,440 Nm/rad
	wrist	Calculated 603 Nm/rad

V. IMPLEMENTATION AND PERFORMANCE VALIDATION

Fig. 11 (a) shows the developed manipulator LIMS. The lengths of upper arm and lower arm are 400 mm, and a dummy hand is mounted at the end of the wrist. For 3-DOF shoulder actuation, three identical hollow-shape joints using capstan drive mechanism are developed. The actuators for the elbow and wrist are mounted at the shoulder as in Fig. 11(b), and they have belt transmission to achieve an additional reduction ratio in addition to the reduction by the tension amplifying mechanism. 50W and 70W MAXON EC45 flat motors were used, which have higher torque than other line-ups, but the rotor inertia is several to ten times higher than the others with similar specs.

Table I contains the design parameters for the proposed mechanism, and Table II shows selected important specifications of the LIMS. As noticed in this table, LIMS was designed to have sufficient joint torque and stiffness for control. For instance, the measured stiffness of the elbow is 1,440 Nm/rad, which is about four times greater than humans (350Nm/rad). It is smaller than the calculated stiffness 2,420 Nm/rad by using (12). This difference is considered to come from the frame flexibility and the elasticity of the extra wires in the actuators. Especially, the 3D-printed ABS links can cause substantial compliance.

Fig. 11 (a) compares the inertias of an industrial robot, human, and LIMS. The inertia for shoulder rotation is comparable to the human inertia, but in the case of the elbow and wrist, the difference is not small. Fig. 11 (b) shows the main reason for the difference. The reflected inertia of the motor rotor is 59% of the elbow inertia and 94% of the wrist inertia, which means that further improvement is possible by selecting the proper motor type.

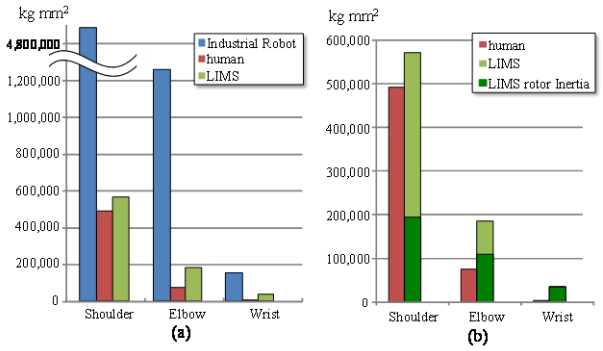

Fig. 12. The comparison of rotational inertia

VI. CONCLUSION AND FUTURE WORK

This paper introduced a unique manipulator that has low mass and inertia without losing stiffness and payload performance. The effectiveness of the proposed tension amplifying mechanism was thoroughly analyzed in terms of stiffness and strength characteristics.

For future research, detailed experiments to verify the performance and safety of the manipulator will be performed, and optimizations of the mechanism, such as replacing motors for lower rotor inertia, will be continued. Also the utilization of collision and impact as the means for communication and collaboration with humans will be investigated.

REFERENCES

[1] M. Zinn, O. Khatib, B. Roth, and J. K. Salisbury, "Playing it safe," IEEE Robotics & Automation Magazine, vol. 11, no. 2, pp. 12–21, 2004.

[2] A. Bicchi and G. Tonietti, "Fast and soft-arm tactics," IEEE Robotics and Automation Magazine, vol. 11, pp. 22–33, June, 2004.

[3] R. Bischoff, J. Kurth, G. Schreiber, R. Koeppe, A. Albu-Schaeffer, A. Beyer, O. Eiberger, S. Haddadin, A. Stemmer, G. Grunwald, and G. Hirzinger, "The KUKA-DLR Lightweight Robot arm – a new reference platform for robotics research and manufacturing," 6th German Conference on Robotics (ROBOTIK), pp. 1–8 , June, 2010.

[4] G.A. Pratt, and M. M. Williamson, "Series elastic actuators," IEEE/RSJ Int. Conf. on Intelligent Robots and Systems (IROS), pp. 399-406, vol.1, 1995.

[5] S. Wolf O. Eiberger and G. Hirzinger, "The DLR FSJ: Energy based design of a variable stiffness joint", IEEE Int. Conf. on Robotics and Automation (ICRA), pp.5082 -5089 2011.

[6] C. Cho and S. Kang, "Design of a Static Balancing Mechanism for a Serial Manipulator With an Unconstrained Joint Space Using One-DOF Gravity Compensators," IEEE Transactions on Robotics, Vol. 30, Issue 2, pp. 421 – 431, 2014.

[7] A.S. Shafer and M.R. Kermani, "On the Feasibility and Suitability of MR Fluid Clutches in Human-Friendly Manipulators," " IEEE Trans. on Mechantronics, Vol. 16, Issue 6, pp. 1073-1082, 2011.

[8] T. Lens and O. von Stryk, "Investigation of safety in human-robot interaction for a series elastic, tendon-driven robot arm," IEEE/RSJ Int. Conf. Intelligent Robots and Systems (IROS), 2012.

[9] Y.-J. Kim, J. Kim, J.-W. Lee, K.-M. Park, K.-S. Roh and J.-Y. Choi, "A Highly Backdrivable Robotic Hand with Sensorless Contact Force Measurements,"IEEE/RSJ Int. Conf. on Robotics and Automation (ICRA), 2014.

[10] K. P. Tee, E. Burdet, C. M. Chew, and T. E. Milner, "A model of force and impedance in human arm movements," Biological Cybernetics, vol. 50, no. 5, pp. 368-375, May 2004.

[11] J. Lee, Y.-J. Kim, Y. Lee, S. Roh, et. al, "Tension Propagation Analysis of Novel Robotized Surgical Platform for Transumbilical Single-Port Access Surgery," IEEE/RSJ International Conference on Intelligent Robots and Systems(IROS), 2013.